



Study of modulating opto-electrochemical properties in Suzuki coupled phenazine derivatives for organic electronics

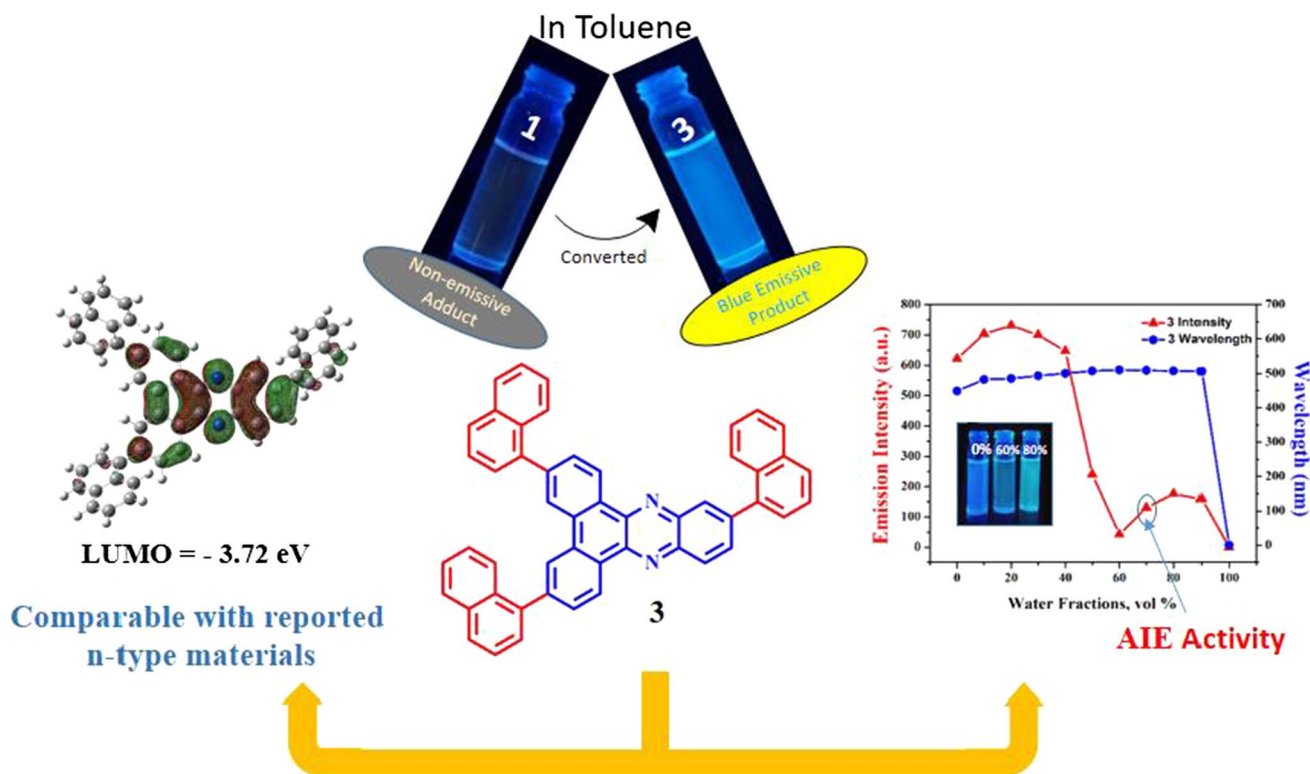
Deepali N. Kanekar¹ · Purav M. Badani¹ · Rajesh M. Kamble¹

Received: 15 February 2021 / Accepted: 1 July 2021
© Institute of Chemistry, Slovak Academy of Sciences 2021

Abstract

In this work, five 3,6,11-trisubstituted-dibenzo[*a,c*]phenazine (**2–6**) derivatives were synthesized by employing Palladium-catalyzed Suzuki–Miyaura ‘C–C bond’ coupling reaction and characterized. Absorption spectra of **2–6** show the formation of charge-transfer complexes. Dyes exhibit blue-green fluorescence with emission maxima 434–506 nm in various solvents and neat solid film. To elucidate AIE phenomenon, photophysical properties of dye **2** and **3** in different THF/water mixture were studied. The HOMO and LUMO energy level were found in the range of –6.38 to –6.82 eV and –3.67 to –3.75 eV with an electrochemical bandgap of 2.71–3.08 eV. The HOMO and LUMO distribution in molecules were further studied by DFT/TD–DFT calculations. Herein, characteristic blue emission, comparable energy levels with n-type materials, and good thermal stability of derivatives make them a potential candidate for their application in optoelectronics.

Graphic abstract



Extended author information available on the last page of the article

Published online: 11 July 2021

Keywords Donor–acceptor system · Suzuki–Miyaura coupling · Photophysical studies · Aggregation-induced emission (AIE) · HOMO and LUMO energy level · n-type materials

Introduction

In the last three decades, tremendous efforts have been put into the development of different organic semiconducting materials due to their various applications as organic light-emitting diodes (OLEDs) (Friend et al. 1999; Baldo et al. 2000), organic field-effect transistors (OFETs) (Anthony et al. 2008), dye-sensitized solar cells (DSSCs) (Grätzel et al. 2009; Imahori et al. 2009), sensors (Jiao et al. 2003; Doré et al. 2004), nonlinear optics (Staub et al. 2003), organic storage media (Zhou et al. 2018), etc. Among the different types (small, polymer, and organometallic) of organic semiconductors, D–A-based small organic molecules drawn considerable research interest because of their notable properties such as well-defined structures, ease of purification, simple structure modulation, good thermal stability, and unique charge transfer properties. These allow tuning of optoelectronic properties through structure modulation/modification. The combination of strong donor and acceptor in the D–A system mostly includes different amines like triarylamine/diarylamine, heterocyclic amines, aliphatic amines as donors, and different N-embedded rings like quinoxaline (Lee et al. 1999; Thomas et al. 2002; Shaikh et al. 2015, 2016a, 2016b; Sharma et al. 2017; Kamble et al. 2018; Kanekar et al. 2019; Singh et al. 2019a, b; Mahadik et al. 2019), pyrazine (Xu et al. 2015a, b; Mahadik et al. 2021), and phenazines (Okamoto et al. 2003; Wang et al. 2013; Shaikh et al. 2016c, 2017; Kanekar et al. 2018, 2020) as acceptor where the use of strong donor and acceptor leads to large charge separation, that is, responsible for strong intramolecular charge transfer (ICT) character in the dye and shifts dye emission at a longer wavelength in the yellow–red region. On the other side, the use of aryl derivatives as a donor in C–C coupled molecules can bring small charge separation in the molecule that leads to weak charge transfer transitions and shifts emission of dye at a shorter wavelength in the blue–green region. Also, it has seen the luminophores that exhibit good emission in dilute solution get quenched on aggregation/in solid state. The development of solid-state emissive materials is necessary for real-world applications (Mullen and Scherf 2006; Furue et al. 2016). Particularly, the blue materials are the key factor that influences the foundation of OLED applications as they can offer a wide gamut RGB (red, green, and blue) color space. Thus, blue materials can be employed as an excitation source to activate emissions of other colors through energy transfer (Hung et al. 2002; Qin et al. 2015). However, compared to orange-red luminophores blue-green luminophores are rare as they face problems such as low efficiency, short lifetime, aggregation

caused quenching, and relatively high-cost processing (Chi and Chou 2010; Huang et al. 2014).

On the other side, the charge transfer property of dye is also an important aspect to consider for its application in optoelectronics. According to past reports, the development of electron-transporting (n-type) materials is lagging much behind compared to hole-transporting materials (p-type) due to their difficult synthesis and instability in the presence of moisture (H₂O) and oxygen (O₂). However, n-type materials are an indispensable component of the electronic circuit (Meijer et al. 2003; Zhou et al. 2014) and need to get synthesized for the development of organic electronics.

To meet the mentioned need for efficient luminescence and electron transport, several strategies are used in the literature. For example, the incorporation of electronegative heteroatoms like N or S to acceptor core or introduction of electron-withdrawing groups such as –F, –CN, –Cl, –NO₂, –COOH, –CF₃, perfluorinated alkyl chain in hole-transporting materials can help to convert p-type material to n-type material (Winkler and Houk 2007). Nonetheless, the ability of the D–A system to induce a twist in the structure of the molecule helps to tackle the problem of aggregation quenching. These molecules restrict intramolecular rotation, thus prevent the formation of detrimental species like exciplexes and excimers and enable molecules to emit in aggregation/solid-state (Furue et al. 2016). Additionally, the introduction of bulky donor groups or integration of AIE units to conventional ACQ fluorophores has been an effective approach to solve the ACQ problem and can induce luminescence into new fluorophores (Yuan et al. 2010).

Therefore, by considering these specific demands of the photophysical and electrochemical characteristics of organic fluorophores, we have designed and synthesized C–C-coupled D–A-based benzo[*a,c*]phenazine derivatives by Suzuki–Miyaura coupling reaction (Miyaura et al. 1981, 2002; Negishi et al. 2002). Herein, phenazine acts as an efficient acceptor core due to the presence of two electron-withdrawing N-atoms in the tricyclic system and the extended conjugation. Among the different electron-deficient azaacenes core, very few reports have appeared on the development of phenazines and their derivatives in optoelectronic applications. This suggests the necessity of its investigation and scope in the development of phenazine derivatives in organic electronics. More specifically, the available reports on acceptor moiety dibenzo[*a,c*]phenazines in the literature include dihydrophenazine derivatives (Okamoto et al. 2003; Zheng et al. 2014), electroluminescent D–A-based dibenzophenazines as hole transporters (Shaikh et al. 2016b), D–A–D-based red dibenzo[*a,c*]phenazine

fluorophores (He et al. 2015), tetrabranched dibenzophenazine derivatives (Boxi et al. 2018), and the recent research on the analysis of ITO surface modified with self-assembled dibenzophenazine carboxylic group (Havare 2020).

Taking the ability to tune the optoelectronic properties of an organic molecule through simple molecular modulation into account, herein we studied the effect of the modified structural framework of dibenzo[*a,c*]phenazine derivatives obtained by attaching different aryl donors at 3rd, 6th, and 11th position of acceptor dibenzo[*a,c*]

phenazine (**1**) core through C–C coupling on photophysical and electrochemical properties. In this structure assembly, the occurrence of charge transfer at a shorter wavelength has expected so that dyes can exhibit emission in the blue-green region. Further, the effect of substitution with electron-donating (EDG) –OCH₃ and withdrawing (EWG) –CN group on peripheral aryl segment on the optoelectrochemical properties such as intramolecular charge transfer transition (ICT), HOMO–LUMO energy levels and band gap has been studied. The structures of synthesized molecules **2–6** are shown in Fig. 1.

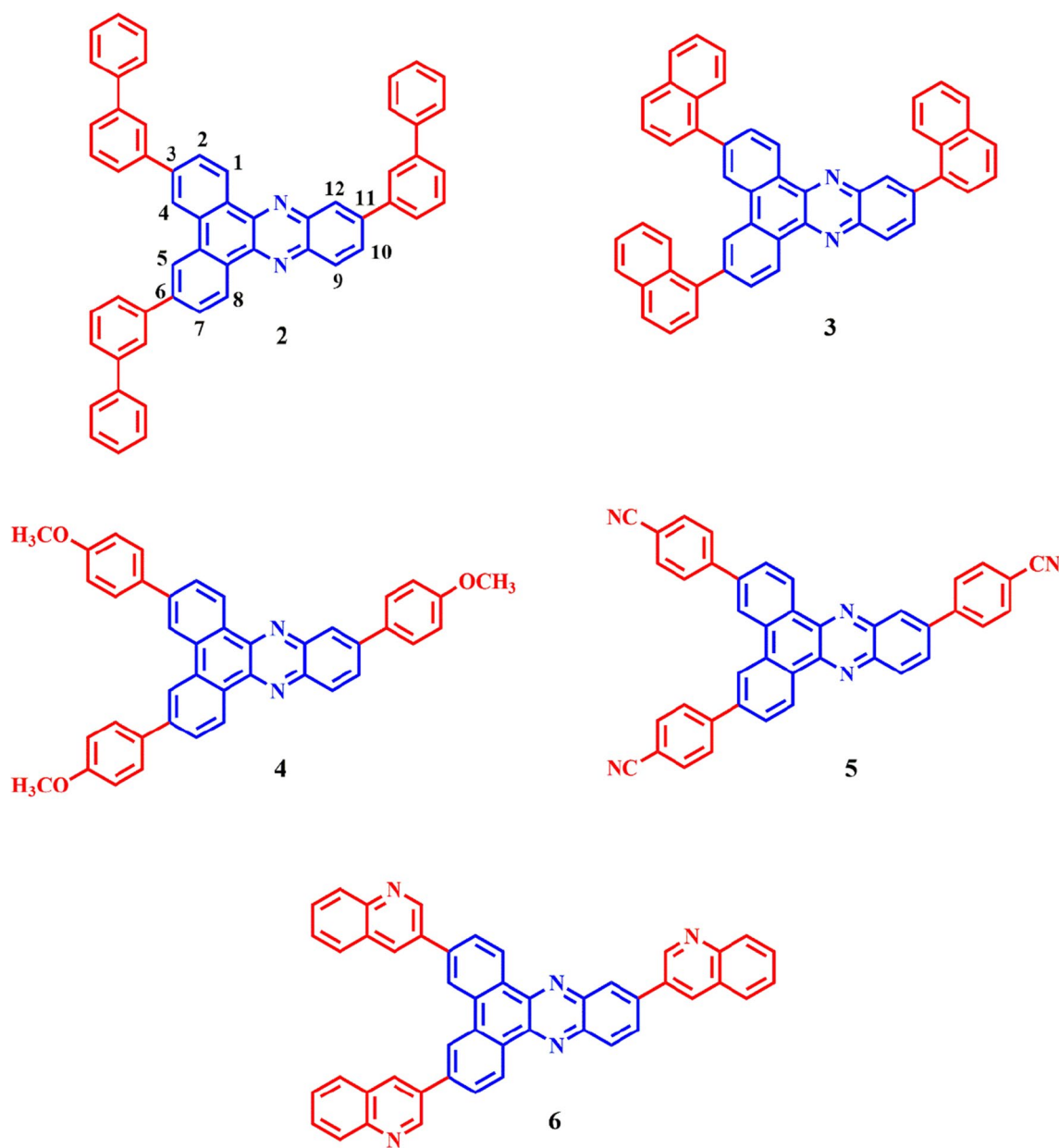


Fig. 1 Molecular structure of compounds **2–6**

Results and discussion

Synthesis and characterization

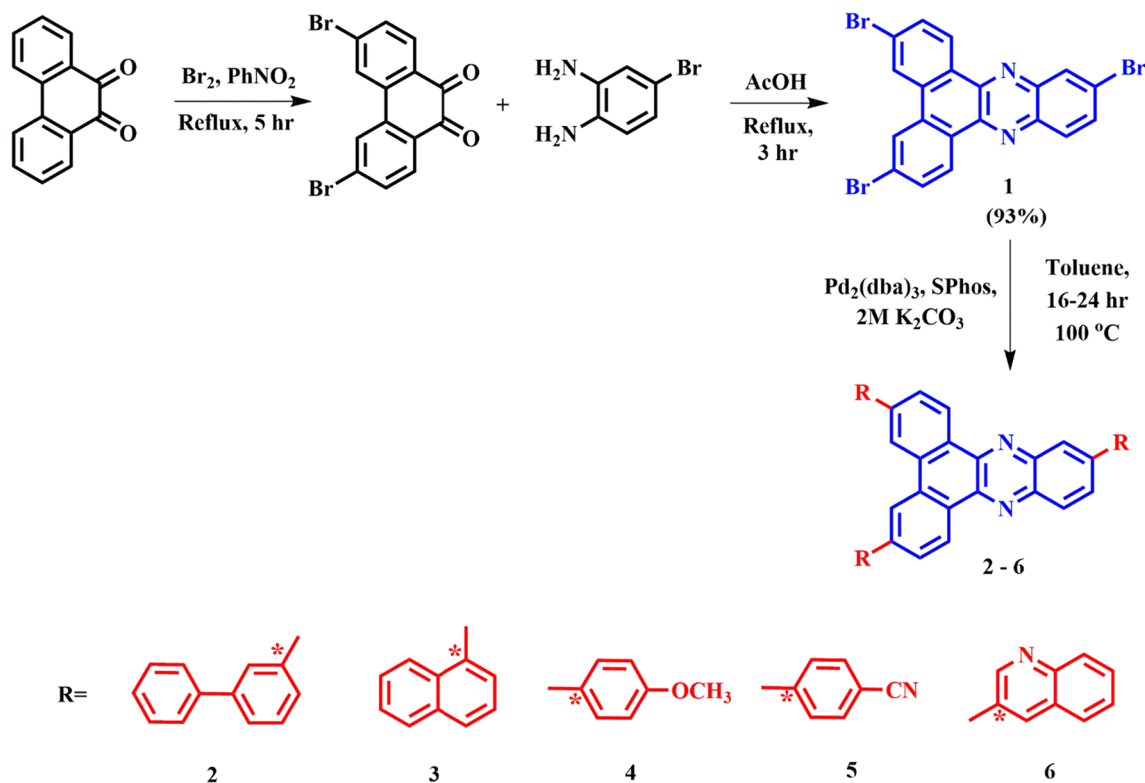
Compound **1** was prepared according to the reported procedure (Shaikh et al. 2017, Xie et al. 2020) and confirmed by MALDI-TOF. Compounds **2–6** were obtained by Suzuki–Miyaura coupling reaction (Miyaura et al. 1981, 2002; Negishi et al. 2002) of **1** with the corresponding aryl boronic acid in the presence of $\text{Pd}_2(\text{dba})_3$ catalyst and SPhos ligand in a mixture of aqueous 2 M K_2CO_3 and toluene (1:3). The synthesized compounds **2–6** were obtained in moderate 30–50% yield as greenish-red solids soluble in common organic solvents including toluene, dichloromethane (DCM), chloroform, tetrahydrofuran (THF), dimethyl sulfoxide (DMSO). However, they are completely insoluble in water. These target molecules were characterized by various spectroscopic technique such as FT-IR, ^1H , ^{13}C -NMR spectroscopy, MALDI-TOF mass spectrometry, and elemental analysis. The synthetic route of compounds **2–6** is shown in Scheme 1.

Photophysical Properties

The photophysical properties of **2–6** were investigated in various solvents and neat solid film by using UV–Visible and fluorescence spectroscopy in order to understand the optical profile of dyes and their alteration due to changing polarity of solvents (toluene, chloroform, DCM, and DMSO) and in a neat solid film. The UV–Vis absorption spectra of compounds **2–6** in toluene and DCM are presented in Fig. 2a and b, while the pertinent data are summarized in Table 1 (See supporting information (SI): Figure S1). The transitions around 282–408 nm in absorption spectra of parent 3,6,11-tribromodibenzo[*a,c*]phenazine (**1**) correspond to $n-\pi^*$ and $\pi-\pi^*$ transitions (Figure S1a and Table S1).

Similarly, the multiple overlapping bands observed in absorption spectra of **2–6** in the above-mentioned solvents at 254–336 nm due to $n-\pi^*$ and $\pi-\pi^*$ transitions occurring in the entire molecule whereas the lower energy band around 372–439 nm found to be affected due to modulating peripheral aryl segment, could be assigned to charge transfer (CT) transitions from peripheral aryl donor to an acceptor phenazine as core (Misra and Bhattacharyya, 2018).

To understand the effect of different aryl donors, optical properties of derivatives were compared within with derivative **2**. The notable redshift of 10–13 nm for CT transitions in **4** attributed to increased donating strength of donor due to



Scheme 1 Synthetic route of **2–6**

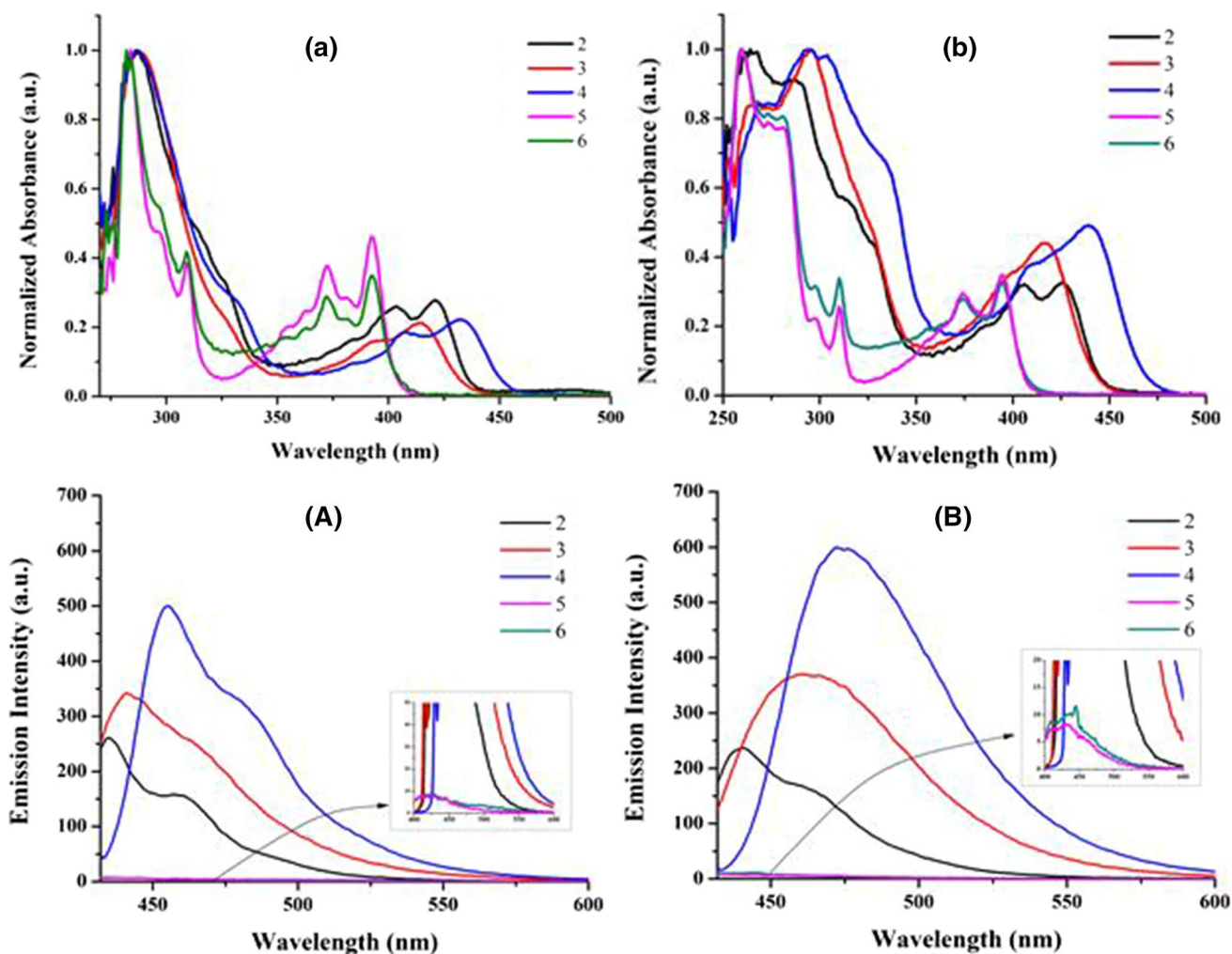


Fig. 2 UV – Vis absorption (above) and emission spectra (below) of compounds 2–6 in toluene (a) and (A) and dichloromethane (b) and (B)

the presence of electron-donating–OCH₃ group in the molecule. Equally, the hypsochromic shift of 25–32 nm in **5** and **6** has been observed which can relate to the presence of strong electron-withdrawing–CN group and quinoline, respectively. However, the absorption maxima of all the molecules possess good molar absorptivity in solution and are found to be unaffected by solvent polarity. This indicates that the dipole moment of the ground state remains unaffected on increase in solvent polarity (Lakowicz 2006). The optical band gap of all derivatives obtained from the offset wavelength was derived from the low energy absorption band and is in the range of 2.64–3.08 eV which is comparable with the optical band gap of reported blue-emitting organic semiconductors (Misra et al. 2004).

The other photophysical factors such as emission data, optical band gap, Stoke's shift, and quantum yield are calculated and summarized in Table 1. The emission spectra of 2–6 were obtained on excitation at their CT maxima. Dyes 2–4 exhibit blue–cyan blue fluorescence with emission

maxima in the range 434–497 nm in toluene, chloroform, DCM, and DMSO (Fig. 2a and b and SI Figure S2). Emission spectra of compounds in various solvents display bathochromic shift of 21–49 nm in compound **4** that could be attributed to the presence of electron-donating –OCH₃ in group on peripheral phenyl segment. Conversely, the emission of dyes **5** and **6** was considerably quenched throughout the solution, suggests inefficient interaction between donor segment and acceptor core that might be due to the presence of electron-withdrawing–CN group on donor entity in **5** and poor electron-donating strength of quinoline in **6**. Blue-shifted emission for low emitting dye **5** and **6** compared to **2** can be observed in the inset (Fig. 2a and b) and witnesses the effect of electron-withdrawing group (–CN group and quinoline) on emission.

The shift in emission maxima of dyes has been observed on changing solvent and suggests the sensitivity of emission of dyes toward the environmental factors of solvents. The noticeable bathochromic shift on increasing polarity

Table 1 UV–vis and photoluminescence (PL) spectroscopic parameters of **2–6** in solution and neat solid state

Compound ^a	Medium	UV–vis	$(E_g^{\text{opt}}, \text{eV})^c$	PL		Stoke's shift, (cm ⁻¹) ^e
		λ_{max} (nm), (log ϵ_{max}) ^b		λ_{em} (nm)	$(\phi_F)^d$	
2	Toluene	282 ^(5.34) , 404 ^(4.76) , 422 ^(4.82)	2.86	434, 459	0.15	655, 1910
	CHCl ₃	289 ^(5.40) , 403 ^(4.99) , 418 ^(4.99)	2.82	442, 465	0.26	1299, 2241
	DCM	281 ^(5.43) , 402 ^(4.76) , 419 ^(4.77)	2.83	441, 463	0.20	1191, 2268
	DMSO	264 ^(6.00) , 289 ^(5.35) , 406 ^(4.90) , 426 ^(4.91)	2.78	448, 471	0.07	1152, 2242
	FILM	292, 368, 412, 433	2.67	487	–	2560
3	Toluene	284 ^(5.73) , 395 ^(4.88) , 414 ^(5.06)	2.84	441	0.22	1478
	CHCl ₃	294 ^(5.35) , 394 ^(4.85) , 413 ^(4.96)	2.84	460	0.46	2474
	DCM	263 ^(5.65) , 294 ^(5.45) , 392 ^(4.99) , 413 ^(5.12)	2.79	461	0.39	2521
	DMSO	293 ^(5.46) , 296 ^(5.47) , 417 ^(5.12)	2.68	496	0.23	3819
	FILM	304, 411, 434	2.67	506	–	4568
4	Toluene	281 ^(5.38) , 330 ^(5.45) , 408 ^(4.61) , 432 ^(4.77)	2.74	455, 482	0.39	1170, 2401
	CHCl ₃	291 ^(5.64) , 329 ^(5.72) , 407 ^(5.15) , 431 ^(5.22)	2.71	474	0.49	2105
	DCM	268 ^(5.43) , 292 ^(5.51) , 328 ^(5.77) , 405 ^(5.46) , 432 ^(5.13)	2.71	475	0.48	2095
	DMSO	294 ^(5.48) , 304 ^(4.97) , 336 ^(5.83) , 407 ^(5.04) , 439 ^(5.16)	2.64	497	0.42	2658
	FILM	304, 418, 437	2.62	499	–	2843
5	Toluene	282 ^(5.43) , 311 ^(5.56) , 372 ^(5.57) , 393 ^(4.96)	3.08	420	0.00095	1653
	CHCl ₃	254 ^(6.00) , 311 ^(5.35) , 373 ^(5.01) , 393 ^(5.06)	3.05	422	0.0015	1748
	DCM	280 ^(5.65) , 309 ^(5.23) , 372 ^(5.14) , 392 ^(5.21)	3.07	424	0.0012	1925
	DMSO	258 ^(6.00) , 310 ^(5.20) , 374 ^(5.12) , 394 ^(5.18)	3.04	436	0.0021	2444
	FILM	314, 380, 402	2.92	430	–	1691
6	Toluene	309 ^(5.61) , 372 ^(5.14) , 393 ^(5.23)	3.07	420	0.0027	1653
	CHCl ₃	254 ^(6.00) , 309 ^(5.27) , 373 ^(5.26) , 393 ^(5.33)	3.06	422	0.0031	1748
	DCM	309 ^(5.15) , 372 ^(5.12) , 392 ^(5.20)	3.08	427	0.0015	2091
	DMSO	310 ^(5.95) , 374 ^(5.02) , 394 ^(5.09)	3.04	438	0.0014	2549
	FILM	380, 400	2.90	451	–	2827

^aRecorded in 10⁻⁶ M solution^blog ϵ_{max} molar absorptivity in solution (M⁻¹ cm⁻¹)^cOptical band gap estimated using offset wavelength derived from the low energy absorption band ($E_g^{\text{opt}} = \frac{1240}{\lambda_{\text{abs edge}}}$) eV^dQuantum yield with reference to fluorescein ($\phi = 0.79$ in 0.1 M NaOH)^eStoke's shifts calculated according to the equation $\Delta\nu = (1/\lambda_{\text{abs}} - 1/\lambda_{\text{em}}) \times 10^7$ (cm⁻¹)

The very low-intensity emission maxima of dyes are in bold.

of solvent from toluene to DMSO correspondingly shifts fluorescence of **2–4** from pure blue (λ_{Emax} : 434–482 nm) to blue–cyan blue region (λ_{Emax} : 448–497 nm) and indicates the decrease in the energy gap (ΔE) between the ground state and the excited state gradually with the increase in the solvent polarity. This redshift in the emission of dyes from non-polar toluene to polar DMSO also suggests the transition in the manifestation of emission from the lowest excited state (LE) to charge transfer state on photoexcitation (Fig. 3b). One can easily see the bathochromic shift in emission obtained on increasing polarity of solvent for dyes through Fig. 3a and b (Reichardt 2002). Though all three dyes (**2–4**) exhibit a bathochromic shift in the emission with an increase in solvent polarity, their solute–solvent interactions slightly differ. To comprehend the polarity effect of

dyes in various solvents, we evaluated Lippert–Mattaga's plot (Mattaga et. al 1956; Lippert 1957) and Weller's plot (Weller 1956) of dyes. Lippert–Mattaga plot (Fig. 3c) is the plot of Stoke's shift vs orientation polarizability (Δf) which only accounts for general solvent effects and not for specific solute–solvent interaction such as π -electron involving (π - π , π -cation, π -anion) or hydrogen-bonding interaction. Lippert–Mattaga plot of dyes **2**, **3**, and **4** suggests that dye **3** and **4** are more sensitive to solvent polarity than dye **2**. However, deviation from the general solvent effect indicates the possibility of specific solute–solvent interaction such as H-bonding of dyes in chloroform and dichloromethane. Further, Weller's plot Fig. 3d which is a graph of emission maxima intensities ($\lambda_{\text{em max}}$) in cm⁻¹ versus Weller's function (Δf_w) shows evident charge transfer in an excited state

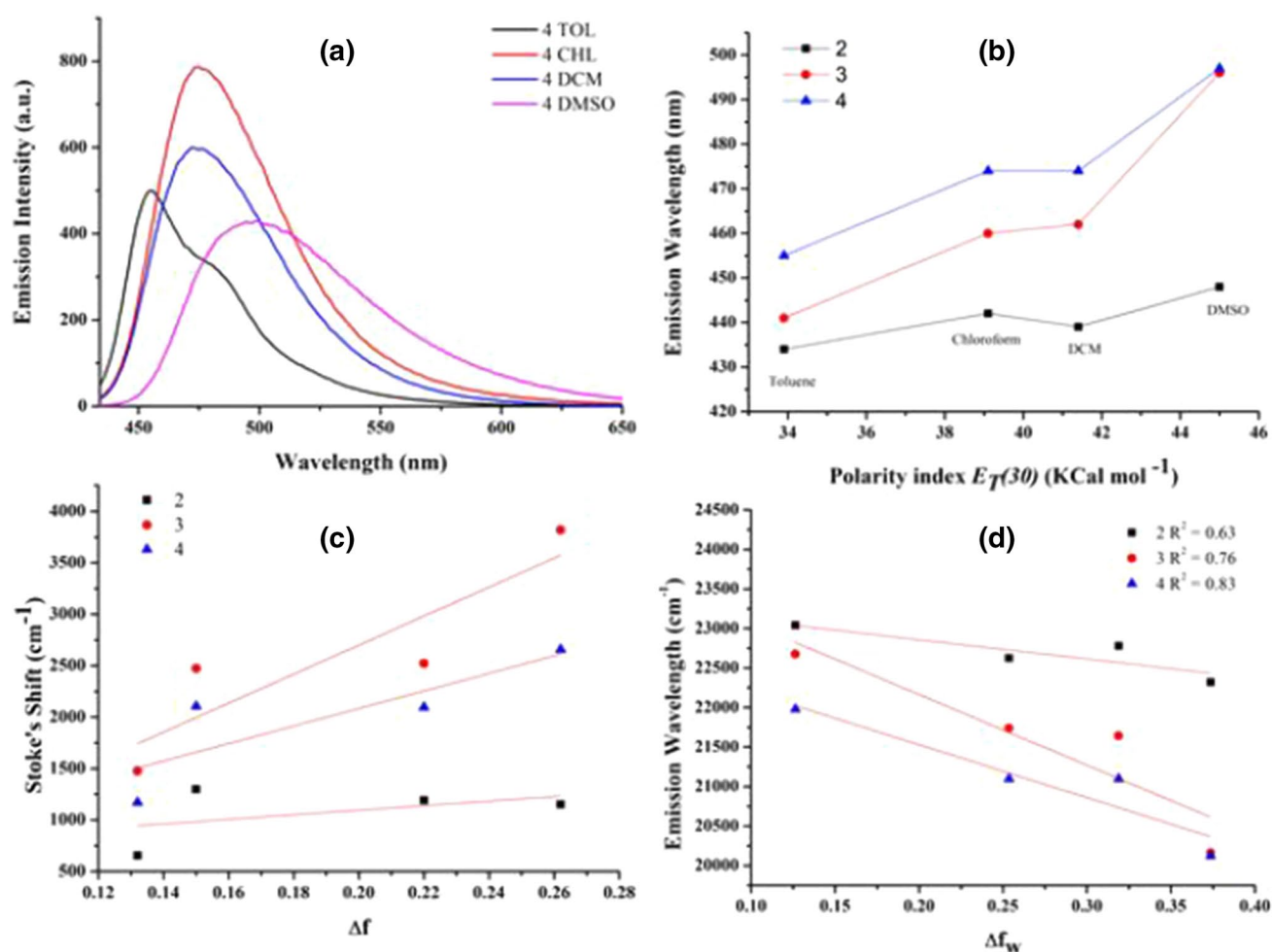


Fig. 3 Solvent polarity effect of dyes 2, 3 and 4 in various solvents viz Toluene, chloroform, dichloromethane and DMSO on emission; **a** Emission spectra of 4 in various solvents, **b** dependence of emission maxima of 2, 3, and 4 on polarity parameters ($E_{T(30)}$) of solvents, **(c)**

plot of Stoke's shift versus orientation polarizability of solvents (Δf), **(d)** plot of emission wavelength of 2, 3, and 4 versus Weller functions (Δf_w)

for D-A-based molecule. Weller's plot of dyes 2–4 demonstrates a linear relationship with good regression coefficient R^2 (0.63 for dye 2, 0.76 for dye 3, and 0.83 for dye 4). It reveals the occurrence of charge transfer from peripheral donor segment to acceptor phenazine core which leads to increased dipole moments of excited state compared to the ground state in polar solvents.

The quantum yield of fluorophore 2–6 in various solvents was estimated by using fluorescein ($\Phi = 0.79$ in 0.1 M NaOH) as a reference (Table 1). The quantum yield of synthesized dyes 2–4 was found in the range 0.07–0.49 in toluene, chloroform, DCM, and DMSO wherein comparatively better quantum yields have been recorded in chloroform and dichloromethane for dyes 2–4 which could be attributed to specific solute–solvent interaction that decreasing rate of non-radiative decay or to a conformational change in fluorophore (Lakowicz 2006). Besides this, quantum yields of

low emitting dye 5 and 6 are less than 0.01. Additionally, derivatives exhibit Stoke's shift in the range 655–3819 cm⁻¹ in various solvents.

Photophysical properties in solid state

To study optical properties in the solid state, a neat solid film of dyes was fabricated by a spin coating of dye solution in chloroform on a quartz plate (see an experimental section for details). The absorption and emission spectra of 2–6 in the solid film are presented in Fig. 4. Likewise in solution, the absorption spectra of 2–6 in the neat solid film display the high energy $n-\pi^*$ and $\pi-\pi^*$ transitions around 292–314 nm, and the transition observed at a longer wavelength from 368 to 437 nm can be assigned CT transitions in the molecule (Table 1). Herein, the absorption profiles observed were broad and slightly red-shifted as compared to solutions

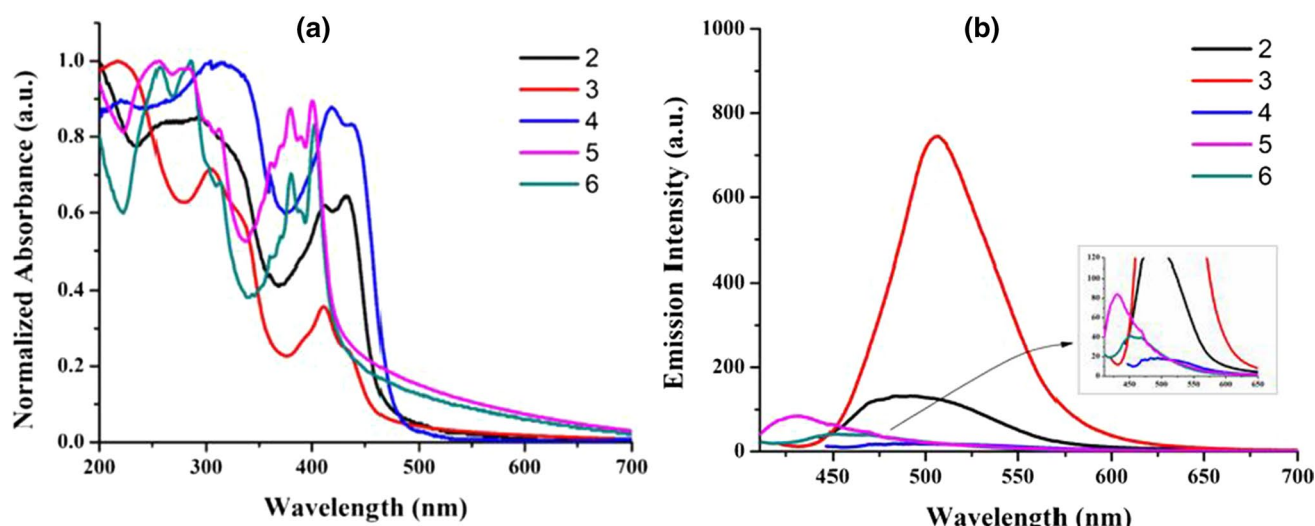


Fig. 4 Absorption **a** and emission spectra **b** of compounds **2–6** in a neat solid film

which can be attributed to the molecular aggregation of dyes on the surface of the film. On the other side, this molecular aggregation was responsible for the decrease in luminescence in dyes **2–6** except **3** wherein lowered emission intensity was recorded for **2** and **5**. A considerable quenching of emission of **4** and **6** has been observed in a solid film. Such aggregation caused quenching in the solid state is a result of fast inter-chain electron transfer via close spatial contact between the molecules (Sun and Sariciftci, 2005).

The varying donating strength of peripheral aryl units tunes the fluorescence in **2–6** from the blue to the green region (λ_{Emax} : 430–506 nm). In emission spectra of **2–6** in neat solid film, though some of the derivatives show weak emission, the effect of modulating donors is distinguishable. Dye **3** own noticeable redshift of 19 nm compared to **2** could be attributed to effective conjugation of naphthalene ring. Similarly, redshift (12 nm) of emission for dye **4** can be assigned to the presence of the electron-donating $-\text{OCH}_3$ group. On the other side, the use of cyanobenzene and quinoline as a donor, blue-shifted emission with 57 nm in **5** and 36 nm in **6** compared to **2** is due to the electron-withdrawing effect of the $-\text{CN}$ group present on phenyl moiety in **5** and quinoline in **6**. Additionally, fluorophores hold good Stoke's shift in the range $1691\text{--}4568\text{ cm}^{-1}$ in a solid film. Further, the luminescence property of dyes in a solid/aggregate state has been explored with AIE studies. For which we have selected molecules **2** and **3**, those have good emission throughout in solution as well as in solid state to understand aggregation effect on the emission of dyes.

Aggregation effect on emission:

Preliminary to understand aggregation effect of **2** and **3**, the THF/water mixtures (0–100%) of respective dyes have

been prepared by reported method to form nanoparticles of organic compounds (Kasai et al. 1992). The dye was first dissolved with THF as it is completely soluble in it, and then, to this solution non-solvent water was slowly added to obtain (10^{-5} M) suspension of aggregates.

These THF/water mixtures of compounds were observed under 365 nm UV illumination in which the quenching of emission at higher water fraction has observed in **2**, whereas emission in case of **3** was considerably recovered at higher water fraction (Fig. 5). This suggests the occurrence of ACQ in **2** that corresponds to its more planar geometry, wherein **3** recoveries of emission at higher water fraction indicate the presence of AIE activity (Birks 1970; Hong et al. 2011). Thus, in order to understand this behavior of dye molecules we have recorded the photoluminescence (PL) intensities of THF/water mixtures of dyes.

The photoluminescence (PL) spectra of **3** in different THF/water fractions are presented in Fig. 5a (for **2** see SI, Figure S3). The emission obtained in pure THF was attributed to CT from the peripheral donor segment (biphenyl/naphthalene) to acceptor phenazine core. Further, gradual addition of water to THF increases the polarity of the solution that bathochromically shifts emission from blue to cyan blue that indicates the occurrence of solvatochromism.

The distinct change in fluorescence on the addition of a small quantity of water in **3** displays better sensitivity of dye for change of medium with water (Otsuki et al. 1993; Jung et al. 2016). Thereafter, the insolubility of dye in water is responsible for lowering in emission intensity on increasing water fraction from 50% f_w which further considerably gets quenched at 60% f_w . Further, the addition of water shows a recovery of fluorescence in the case of **3** from 70 to 90% f_w (Fig. 5b). This suggests the formation of nano-aggregates that are responsible for improved

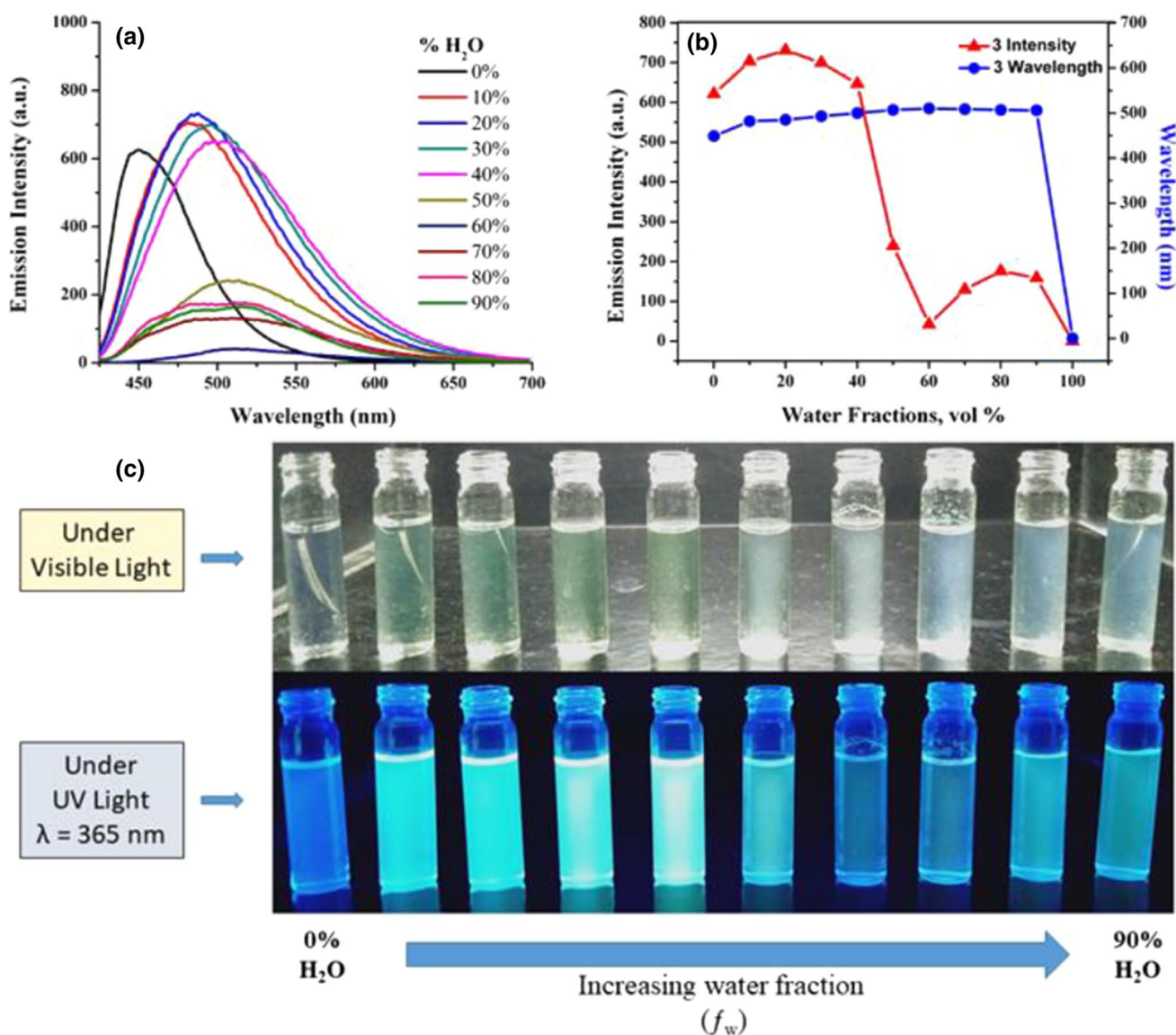


Fig. 5 Fluorescence spectra of **3** **A**, plots of PL intensity and peak wavelength versus water fractions (f_w) **B**, and photographs of **3** in THF—water mixture with increasing water fractions (f_w) **C**

emission, well known as AIE. In AIE, the formation of nano-aggregates restricts the non-radiative decay process such as intramolecular rotation and vibration and makes luminogen emits efficiently (Hong et al. 2011). The varying emission intensity of nanosuspension was attributed to a different physical constraint of molecule and yield of nanoparticles obtained in nanosuspension (Liu et al. 2018). The AIE behavior of dye was further explored using absorption spectroscopy (see SI, Figure S4). In absorption spectra, level off the tail or Mie scattering at a longer wavelength above 50% f_w in **3** is the consequence of scattering of light by nanoparticles formed in

suspension (Tong et al. 2006). This confirms the presence of AIE at a higher water fraction due to the formation of nanoparticles.

To confirm the formation of nano-aggregates at higher water fractions and to understand the size and morphology of aggregates, we subjected suspension of luminophore **3** in THF/water mixture of 80% f_w under a scanning electron microscope (FEG-SEM). The SEM image of **3** (Fig. 6) in 80% f_w displays that aggregate formed is spherical in nature with a mean diameter of 31–68 nm. The nanosuspension of **3** obtained was quite transparent and stable.

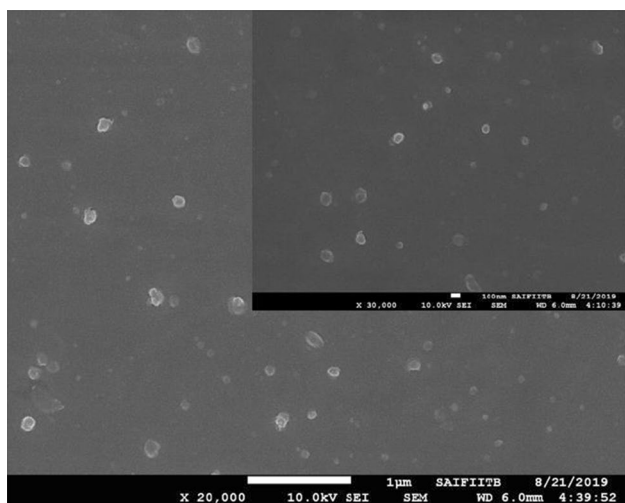


Fig. 6 SEM image of nanoparticles of **3** obtained in nanoparticle suspension containing 80% volume fraction of water (f_w) in THF

Table 2 Electrochemical data of **1–6**

Compound	$E_{\text{oxi}}^{\text{peak a}}$	$E_{\text{red}}^{\text{peak b}}$	HOMO ^c	LUMO ^d	E_g^e
1	–	–0.99, –1.47	–6.51	–3.63	2.88
2	–	–0.92, –1.34	–6.53	–3.70	2.83
3	–	–0.90, –1.32	–6.56	–3.72	2.84
4	–	–0.95, –1.30	–6.38	–3.67	2.71
5	–	–0.89, –1.41, –1.59	–6.82	–3.75	3.07
6	–	–0.95, –1.39, –1.56	–6.76	–3.68	3.08

^a $E_{\text{oxi}}^{\text{peak}}$ oxidation peak potential (V). ^b $E_{\text{red}}^{\text{peak}}$ reduction peak potential (V). ^c HOMO energy level calculated from $E_{\text{HOMO}} = -[E_g^{\text{opt}} - E_{\text{LUMO}}]$ eV. ^d LUMO energy level calculated from $E_{\text{LUMO}} = -[E_{\text{red}}^{\text{peak}} - E_{\text{redox}}(\text{Fc}/\text{Fc}^+) + 5.1]$ eV. ^e $E_g = [\text{HOMO} \cdot \text{LUMO}]$ eV.

Electrochemical properties

The electrochemical propensity and redox potential of the derivatives were examined by cyclic voltammetry in DCM with ferrocene as an internal standard, and the pertinent data are presented in Table 2. The cyclic voltammogram of **2** and **5** is presented in Fig. 7 (for other compounds, see SI Figure S5).

On an anodic sweep, lower intensity of oxidation waves leads to difficulty in the identification of proper oxidation peaks in **1–6**. On the other side, a cathodic sweep of **1–6** displays two predominant quasi-reversible waves that correspond to the reduction in phenazine moiety through the two-electron process (de la Cruz et al. 2020). All the derivatives exhibit nearly similar redox behavior. However, the presence of one extra reduction peak in compounds **5** and **6** could be attributed to the reduction in peripheral cyanobenzene and quinoline moiety, respectively.

It is important to know the HOMO and LUMO energy levels of organic materials for their use in optoelectronics. Thus, the LUMO energy level of **2–6** was calculated by first reduction potential, whereas the HOMO energy levels of **2–6** were calculated from the difference of optical band gap obtained in DCM and LUMO energy values. The calculated HOMO and LUMO energy levels of **2–6** were found in the range –6.38 to –6.82 eV and –3.67 to –3.75 eV. Herein, the values of LUMO energy level below –3.0 eV suggest capability of electron transport (Jones et al. 2007; Gao and Hu 2014) in derivatives with reference to reported n-type materials such as perfluoroalkyl substituted C60-fused N-methylpyrrolidine-para-dodecyl phenyl derivative (C60PC12F25) (LUMO = –3.63 eV) (Chikamatsu et al. 2008), alkyl-substituted poly(benzoquinolinophenanthro

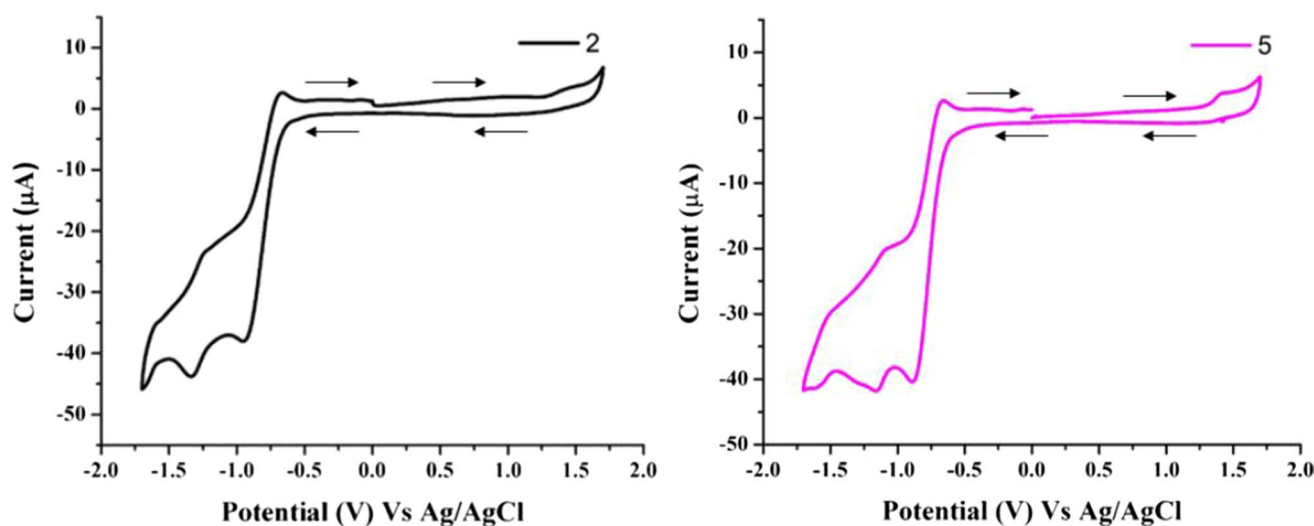


Fig. 7 Cyclic voltammogram (full scan) of compounds **2** and **5** measured in anhydrous dichloromethane

linedione) (PNDI-2BocL) (LUMO = -3.54 eV) (Durban et al. 2011), and N, N'-bis(1*H*,1*H*,2*H*,2*H*-perfluorodecyl)-1,4,5,8-naphthalene tetracarboxylic diimide (8-2-NTCDI) (LUMO = -3.77 eV) (Byung et al. 2010).

Theoretical properties

To take a better insight into the impact of modulating donors at the periphery of acceptor phenazine core on the HOMO and LUMO energy levels of molecules, its electronic structures were computed using density functional theory (DFT) under B3LYP/6-311G basis set within a Gaussian 03 program (Frisch et. al 2004). The optimized geometries and theoretically calculated frontier molecular orbitals of **2** and **4** are presented in Fig. 8 (for other compounds, see SI Figure S22–S33).

The HOMO and LUMO distribution in derivatives depend on its molecular design and are found to be affected due to molecular conformation. It can be observed that in

parent **1** the HOMO and LUMO spread over the entire molecule. However, in **2–6** the peripheral units were joined to central phenazine core by C₁–C₂ bond wherein HOMO is resided linearly on two of the peripheral segment and central core through conjugation, whereas LUMO predominately presents on central phenazine core witness's occurrence of characteristic HOMO–LUMO transitions in these molecules. It is apparent from electronic structures that the non-planarity impairs the electronic coupling at some part of the molecule that leads to an absence of electron density over there. In addition to these, poorly separated HOMO and LUMO energy levels and small dipole moments in the molecules prevail weak charge transfer transition between the donor aryl groups and acceptor phenazine core (Chen et. al 2014). The dipole moments obtained for **4** and **5** are large compared to other derivatives which are attributed to polar –OCH₃ and –CN group on arylamine, respectively.

The computationally calculated energies of the HOMO and LUMO levels, HOMO–LUMO gap, vertical ionization

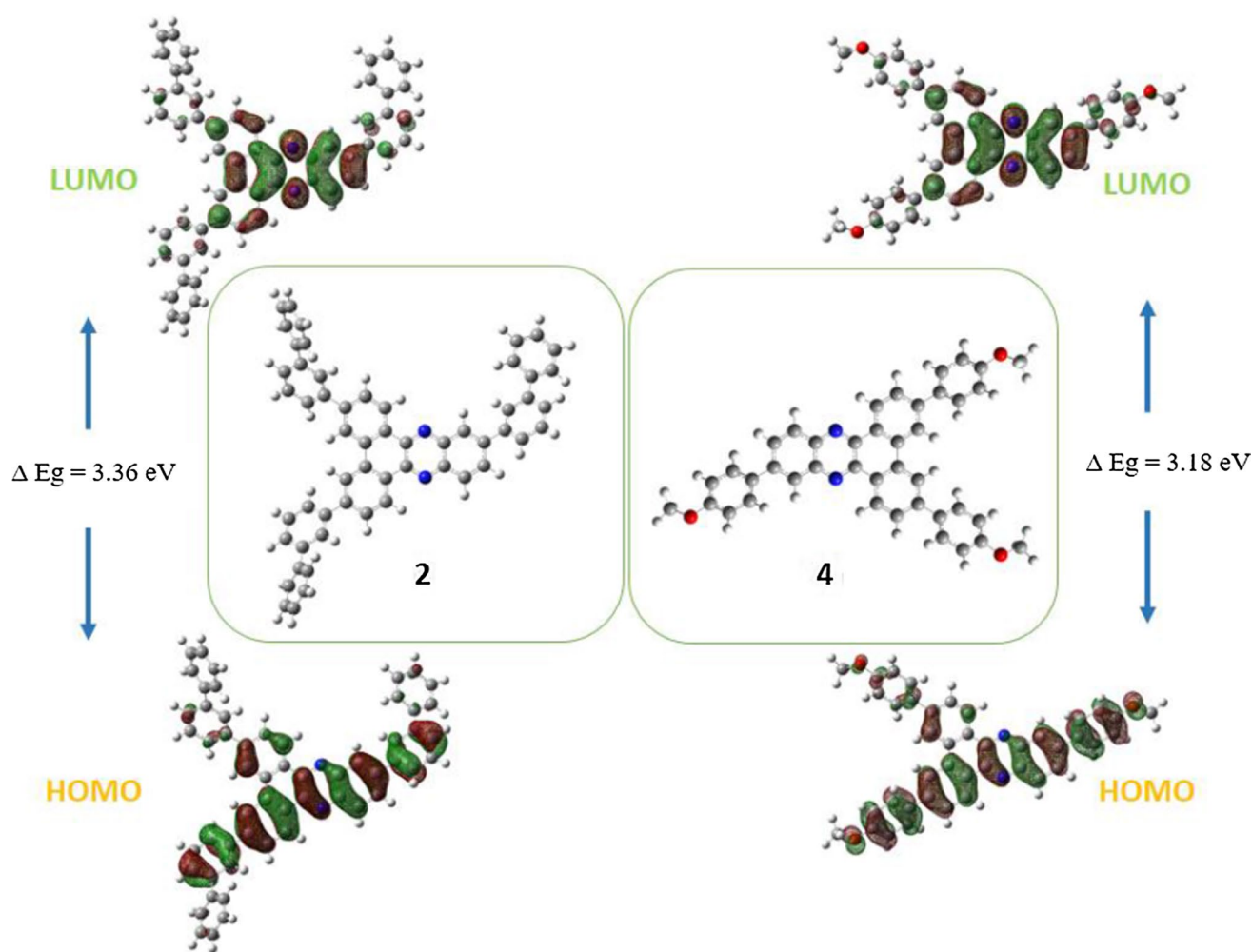


Fig. 8 Optimized structures and Correlation diagram showing Frontier molecular orbitals and energies of **2** and **4**

Table 3 Computed Ionization potentials, electron affinities, wavelengths, oscillator strengths, main vertical electronic transition in the gas phase, orbital energies, and dipole moments of **1–6**

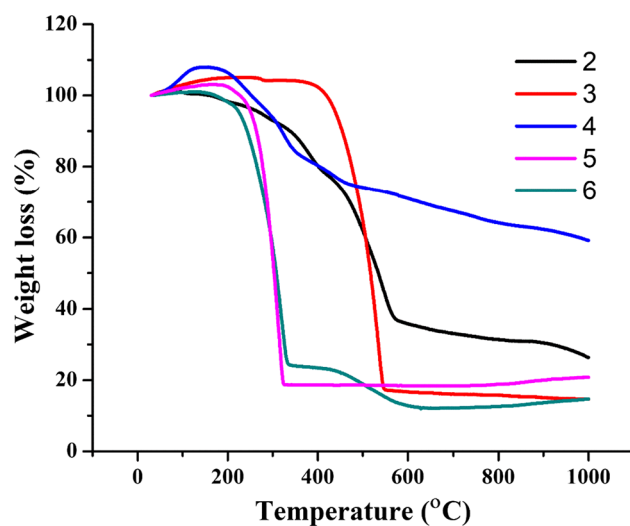
Compound	E_a (eV)	I_p (eV)	λ_{\max} (nm)	F	Assignments	E_{HOMO} (eV)	E_{LUMO} (eV)	E_g (eV)	Dipole (debye)
1	7.93	1.86	397	0.1163	HOMO \rightarrow LUMO (61.22%)	-6.71	-3.14	3.58	1.41
			384	0.0012	HOMO-3 \rightarrow LUMO+1 (70.28%)				
2	6.97	1.62	422	0.4919	HOMO \rightarrow LUMO (68%)	-6.06	-2.70	3.36	0.53
			407	0.1749	HOMO-1 \rightarrow LUMO (66%)				
3	6.81	1.61	443	0.2609	HOMO \rightarrow LUMO (68%)	-5.92	-2.70	3.22	0.53
			427	0.1497	HOMO-1 \rightarrow LUMO (67%)				
4	6.66	1.43	444	0.5985	HOMO \rightarrow LUMO (69%)	-5.72	-2.54	3.18	1.79
			422	0.1241	HOMO-1 \rightarrow LUMO (68%)				
5	7.71	2.31	419	0.5621	HOMO \rightarrow LUMO (67%)	-6.73	-3.35	3.37	4.83
			408	0.2150	HOMO-1 \rightarrow LUMO (66%)				
6	7.14	1.92	428	0.7388	HOMO \rightarrow LUMO (68%)	-6.24	-2.95	3.27	2.00
			412	0.1268	HOMO-1 \rightarrow LUMO (67%)				

potential, electron affinity, and the ground state dipole moment for all derivatives are given in Table 3. The HOMO and LUMO energy of **2–6** is in the range of -5.72 to -6.73 eV and -2.54 to -3.35 eV, respectively. These HOMO values are comparable with experimentally calculated energy levels to some extent, whereas LUMO values show slight deviation with experimentally obtained data. Substitution with different peripheral donor units on parent **1** considerably tunes HOMO and LUMO energy level values. In which, an increase in π -conjugation in donors like biphenyl, naphthyl in **2**, **3**, and strong EDG $-\text{OCH}_3$ group in **4** leads to higher HOMO energy level values. Conversely, the presence of EWG $-\text{CN}$ group and quinoline is responsible for lower LUMO values in **5** and **6**. The computed bandgap for **2–6** gets lowered as compared to parent **1** and is in the range of 3.18 – 3.37 eV. The small bandgap (3.18 eV) in **4** is assigned to strong electron-donating $-\text{OCH}_3$ group on aryl segment.

The transition energies, oscillator strength, and assignment for the most relevant singlet excited states in each of the molecules are given in Table 3, and other assignments are given in supporting information. The first vertical ionization potential (IP) and the electron affinity (EA) were calculated computationally as the difference in the total energies of neutral and cationic/anionic species, respectively. Thereafter, the optical properties were evaluated by TD-DFT in the gas phase using 6-311G basis set (for simulated electronic absorption spectra of **1–6** in the gas phase, see SI Figure S34). The transitions above 350 nm correspond to charge transfer transitions in the dyes and have been affected by modulating peripheral donor segments in the molecule.

Thermal properties

The thermal stability of **1–6** was studied by thermogravimetric analysis (TGA), and the melting point was

**Fig. 9** TGA thermogram of **2–6** under nitrogen atmosphere at normal pressure. Heating rate, 10 °C/min

determined by the open capillary method. The TGA thermogram of **2–6** has been obtained in a nitrogen atmosphere at normal pressure with heating rate, 10 °C/min, and displayed in Fig. 9 (For **1**, see SI Figure S35). The slight increase in mass on the increasing temperature at beginning of the TGA thermogram can be attributed to the buoyancy effect in the TGA system. (Bottom 2008).

However, the TGA thermogram of **2–6** revealed that these dyes exhibit good thermal stability. The decomposition temperature corresponds to 5% and 10% weight losses are found in the range 222 – 438 °C and 243 – 452 °C respectively (Table 4). The order of thermal stability in derivatives **2–6** is **3** > **4** > **2** > **6** > **5**.

Table 4 Thermal properties of compounds 1–6

Compound	1	2	3	4	5	6
TGA						
^a T ₅ (°C)	346	249	438	285	222	250
^a T ₁₀ (°C)	360	329	452	316	243	262

Conclusion

In summary, five C–C-coupled D–A-based phenazine derivatives are synthesized and characterized. It is observed that adduct **1** is non-emissive and electron-deficient, whereas attachment of donor aryl moieties at periphery induces emission in **2–4** derivatives. The absorption and emission spectra were influenced by the nature of peripheral donor aryl moieties and demonstrate the formation of charge-transfer complexes. The resulting luminogen shows weak D–A interaction but characteristic emission in the blue region. The optical band (2.62–3.08 eV) of synthesized dyes well matches with reported blue-emitting organic semiconductors. Further, solvent polarity plots viz. $E_{T(30)}$ vs emission wavelength, Lippert–Mattaga and Weller's models provide the validation of charge transfer (CT) characteristics in a designed D–A system. Aggregation studies of dyes **2** and **3** expose the ACQ in dye **2** and weak AIE in dye **3** wherein the notable change in fluorescence on the addition of water to THF solution of dye **3** reveals its sensitivity for change in medium with water. The FEG-SEM studies unveil the nanoparticles of **3** that get formed at higher water fraction ($f_w = 80\%$ in THF/water mixtures) are spherical in nature with a mean diameter of 31–68 nm. Electrochemical investigation shows that electron-accepting property retains in the derivatives. The HOMO and LUMO are in the range –6.38 to –6.82 eV and –3.67 to –3.75 eV, respectively, and found to be comparable with reported electron-transporting (n-type) materials. DFT and TD-DFT studies verify weak D–A interaction in the molecules through poorly separated HOMO and LUMO energy levels and small dipole moments. Additionally, all the dyes possess good thermal stability. From these results, we believe that the synthesized dyes could be used as blue emitters and electron-transporting (n-type) materials in optoelectronics.

Experimental section

Chemicals and materials

All the starting materials and reagents were purchased from commercial sources (Sigma-Aldrich and Alfa Aesar) and were used without any further treatment and purification unless otherwise mentioned. The organic solvents were of HPLC and spectroscopic grade and were dried and freshly

distilled using the standard procedures and handled in a moisture-free atmosphere. Column chromatography was carried out using SD-fine silica gel (60–120 mesh), eluting with n-hexane and chloroform. The progress of the reaction and the purity of the compound was checked by thin-layer chromatography (TLC) on silica-gel-coated glass plates, in which the spots were visualized with UV light (365 nm) and in an iodine chamber.

Instrumentation and methods

UV–visible spectra were recorded in 10^{-6} mol L⁻¹ solution in a 1 cm path length quartz cuvette as well as the neat solid films on a SHIMADZU UV-2401PC instrument at room temperature. The neat solid film of compounds **2–6** was prepared by using a spin coater (Holmarc HO-TH-05) at 1000 rpm for 2 min ~ 6 mg mL⁻¹ of the sample in chloroform. Quartz plates were used for neat solid film studies. The excitation and emission spectra were carried out on a PerkinElmer LS 55 Fluorescence spectrophotometer. Cyclic voltammetry studies were carried out on a computer-controlled Palmsens3 potentiostat. Typically, a three-electrode cell equipped with a glassy carbon working electrode, an Ag/AgCl (non-aqueous) reference electrode, and platinum (Pt) wire as the counter electrode was employed. The measurements were carried at room temperature in anhydrous dichloromethane with tetra-butyl ammonium hexafluorophosphate solution (0.1 M) as the supporting electrolyte with a scan rate of 100 mVs⁻¹. The potential of the Ag/AgCl reference electrode was calibrated by using a ferrocene/ferrocenium redox couple, which has the known oxidation potential of +5.1 eV. The thermogravimetric analysis (TGA) was performed using a MettlerToledo instrument (TG) under nitrogen atmosphere. ¹H and ¹³C NMR spectra were recorded using CDCl₃ on Varian 300 MHz Ultrashield spectrometer with tetramethylsilane (TMS) as an internal reference at working frequency 300 and 75 MHz, respectively. Fourier transform infrared (FT–IR) spectra were recorded on a PerkinElmer Frontier 91,579. Mass spectrometric measurements were recorded using MALDI–TOF (Bruker), and elemental analysis was carried out on EA Euro–elemental analysis instrument. To confirm the formation of nanoparticles in AIE studies, the sample of synthesized dye was subjected to field emission gun scanning electron microscopy (JEOL JSM-7600F FEG–SEM).

Synthesis procedures

Synthesis of 3,6,11-tribromodibenzo[*a,c*]phenazine (1).

Compound **1** was prepared and obtained according to the reported procedure (Shaikh et al. 2017, Xie et al 2020) as mint green solid. Yield 1.20 g (93%); mp > 250 °C. FT-IR, (KBr, ν_{\max} cm⁻¹): 3070, 1587, 1358, 1054, 825; MALDI-TOF: mass calcd for C₂₀H₉Br₃N₂ [M⁺]: 517.01, found: 518.87; elemental anal. calcd for C₂₀H₉Br₃N₂: C 46.46, H 1.75, Br 46.36, N 5.42. found: C 46.15, H 1.88, Br 46.47, N 5.50.

General procedure for the synthesis of 2–6

Toluene (30 mL) and aqueous solution of K₂CO₃ (2 M, 20 mL) were added to a flask containing a mixture of compound **1** (0.1 g, 0.19 mmol), aryl-boronic acid (0.57 mmol), Pd₂(dba)₃ (20 mg, 0.02 mmol), and SPhos (25 mg, 0.048 mmol). The reaction mixture was continuously stirred under a nitrogen atmosphere at 100 °C for 16–24 h. The reaction mixture was cooled to room temperature and extracted with chloroform (5 × 25 mL), and the solution was then washed with water (5 × 25 mL). All organic layers were combined and dried with anhydrous Na₂SO₄ and evaporated to obtain the dry crude product. To get insight to obtain pure product by column chromatography, the TLC of crude product and reactant was checked before proceeding to separation with column chromatography. Thereafter, the slurry of crude product was made by mixing it with chloroform and silica (60–120 mesh), where the mixture was dried to afford a free-flowing slurry. Silica (60–120 mesh) column was prepared in 100% n-hexane, and slurry of crude product was loaded through n-hexane on the column. Then, the column was run with different ratios of n-hexane/chloroform to obtain purified compounds as green to dark red solids (Compound **2**, **3**, **4**, **5**, and **6** were purified by using n-hexane/chloroform with ratio 80:20, 80:20, 60:40, 60:40, and 70:30, respectively).

3,6,11-tri([1,1'-biphenyl]-3-yl)dibenzo[*a,c*]phenazine (2)

Greenish solid, yield: 70 mg (50%); mp > 250 °C. FT-IR (KBr, ν_{\max} cm⁻¹): 3058, 2923, 2852, 1350, 750, 693; ¹H NMR (300 MHz, CDCl₃) δ 9.37 (dd, *J* = 4.5, 4.5 Hz, 2H), 8.72 (s, 2H), 8.51 (s, 1H), 8.31 (d, *J* = 8.9 Hz, 1H), 8.16–7.91 (m, 6H), 8.16–7.91 (m, 24H); ¹³C NMR (75 MHz, CDCl₃): δ 142.16, 142.14, 142.09, 141.51, 141.06, 140.97, 140.40, 132.18, 129.51, 129.44, 128.90, 127.55, 127.35, 127.26, 126.60, 126.49, 121.53; MALDI-TOF: mass calcd for C₅₆H₃₆N₂ [M⁺]: 736.90, found: 736.31; elemental anal.

calcd for C₅₆H₃₆N₂: C 91.27, H 4.92, N 3.80 found: C 91.18, H 5.02, N 3.80.

3,6,11-tri(naphthalen-1-yl)dibenzo[*a,c*]phenazine (3)

Greenish solid, yield: 60 mg (48%); mp > 250 °C. FT-IR (KBr, ν_{\max} cm⁻¹): 3042, 2928, 1358, 1045, 760; ¹H NMR (300 MHz, CDCl₃) δ 9.58–9.34 (m, 2H), 8.92–8.68 (m, 2H), 8.57 (d, *J* = 16.5 Hz, 1H), 8.44–8.31 (m, 1H), 8.25–7.91 (m, 5H), 7.86–7.32 (m, 19H); ¹³C NMR could not be obtained due to poor solubility, MALDI-TOF: mass calcd for C₅₀H₃₀N₂ [M⁺]: 658.79, found: 658.39; elemental anal. calcd for C₅₀H₃₀N₂: C 91.16, H 4.59, N 4.25 found: C 91.07, H 4.65, N 4.28.

3,6,11-tris(4-methoxyphenyl)dibenzo[*a,c*]phenazine (4)

Red solid, yield: 34 mg (30%); mp > 250 °C. FT-IR (KBr, ν_{\max} cm⁻¹): 3062, 2919, 1596, 1244, 817; ¹H NMR and ¹³C NMR could not be obtained due to poor yield and solubility; MALDI-TOF: mass calcd for C₄₁H₃₀N₂O₃ [M⁺]: 598.69 found: 598.24; elemental anal. calcd for C₄₁H₃₀N₂O₃: C 82.25, H 5.05, N 4.68 found: C 82.37, H 5.16, N 4.72.

4,4',4''-(dibenzo[*a,c*]phenazine-3,6,11-triyl)tribenzonitrile (5)

Green solid, yield: 54 mg (48%); mp 190 °C. FT-IR (KBr, ν_{\max} cm⁻¹): 3051, 2919, 1358, 1026, 760; ¹H NMR (300 MHz, CDCl₃) δ 9.45–9.33 (m, 2H), 8.93 (s, 1H), 8.55 (t, *J* = 6.2 Hz, 2H), 8.47 (s, 1H), 8.39–8.25 (m, 2H), 8.23 (d, *J* = 4.2 Hz, 1H), 7.95–7.66 (m, 12H); ¹³C NMR could not be obtained due to poor solubility; MALDI-TOF: mass calcd for C₄₁H₂₁N₅ [M⁺]: 583.64, found: 583.21; elemental anal. calcd for C₄₁H₂₁N₅: C 84.37, H 3.63, N 12.00 found: C 84.21, H 3.71, N 12.08.

3,6,11-tri(quinolin-3-yl)dibenzo[*a,c*]phenazine (6)

Yellow solid, yield: 52 mg (45%); mp 195 °C. FT-IR (KBr, ν_{\max} cm⁻¹): 3051, 2957, 1263, 1017, 760; ¹H NMR (300 MHz, CDCl₃): δ 9.38 (d, *J* = 7.6 Hz, 2H), 8.93–8.87 (m, 3H), 8.54 (d, *J* = 7.8 Hz, 2H), 8.31 (dd, *J* = 6.4, 3.5 Hz, 2H), 7.92–7.68 (m, 12H), 7.66–7.57 (m, 4H), 7.45–7.36 (m, 2H); ¹³C NMR (75 MHz, CDCl₃) δ 143.32, 142.44, 142.19, 132.05, 130.50, 130.29, 129.73, 129.46, 128.97, 128.39, 127.92, 126.27, 125.43, 122.90; MALDI-TOF: mass calcd for C₄₇H₂₇N₅ [M⁺]: 661.71 found: 662.03; elemental anal. calcd for C₄₇H₂₇N₅: C 85.30, H 4.11, N 10.58 found: C 85.11, H 4.27, N 10.62.

Preparation of nano-aggregates

Stock THF solution of the dyes **2** and **3** with concentration 10⁻⁴ M was prepared. Aliquots of stock solution were transferred to a 5 mL volumetric flask. After dissolving the dye in an appropriate amount of THF, water was added drop-wise

under vigorous shaking to obtain a 10^{-5} M solution with different water contents (0–100 vol%). The photoluminescence (PL) measurement of the resultant solution was recorded. Also, the size and morphology of nanoparticles of dye **3** were observed by field emission scanning electron microscopy (FEG–SEM).

Theoretical calculation

DFT and time-dependant density functional theoretical (TD–DFT) calculations were performed using Gaussian 03 software package using B3LYP as exchange–correlation functional at 6–311G basis set.

Supplementary Information The online version contains supplementary material available at <https://doi.org/10.1007/s11696-021-01772-y>.

Acknowledgements The authors are greatly thankful to the Micro-Analytical Laboratory, Department of Chemistry, the University of Mumbai for providing Instrumental facilities. We sincerely thank the Tata Institute of Fundamental Research (TIFR), Mumbai for providing MALDI-TOF and Sophisticated Analytical Instrument Facility, IIT Bombay for providing FEG-SEM. The author DNK is grateful to DST–PURSE for JRF.

References

- Anthony JE (2008) The larger acenes: versatile organic semiconductors. *Angew Chem Int Ed* 47:452–483. <https://doi.org/10.1002/anie.200604045>
- Baldo MA, Thompson ME, Forrest SR (2000) High-efficiency fluorescent organic light emitting devices using a phosphorescent sensitizer. *Nature* 403:750–753. <https://doi.org/10.1038/35001541>
- Birks JB (1970) *Photophysics of aromatic molecules*. London: Wiley-Interscience, P 1294–1295. <https://doi.org/10.1002/bbpc.19700741223>.
- Bottom R (2008) Thermogravimetric analysis. In: Gabbott P (ed) *Principles and applications of thermal analysis* wiley online books, pp 87–118. <https://doi.org/10.1002/9780470697702.ch3>
- Boxi S, Jana D, Parui PP, Ghorai BK (2018) Dibenzo[*a, c*]phenazine-based donor-acceptor (D–A) tetra branched molecules: fine tuning of optical properties. *ChemistrySelect* 3:6953–6959. <https://doi.org/10.1002/slct.201801500>
- Byung B, Jung J, Lee K, Sun J, Andreou AG, Katz HE (2010) Air-operable, high-mobility organic transistors with semifluorinated side chains and unsubstituted naphthalenetetracarboxylic diimide cores: high mobility and environmental and bias stress stability from the perfluorooctylpropyl side Chain. *Adv Funct Mater* 20:2930–2944. <https://doi.org/10.1002/adfm.201000655>
- Chen L, Jiang Y, Nie H, Hu R, Kwok HS, Huang QFA, Zhao Z, Tang BZ (2014) Rational design of aggregation-induced emission luminogen with weak electron donor-acceptor interaction to achieve highly efficient undoped bilayer OLEDs. *ACS Appl Mater Interfaces* 6:17215–17225. <https://doi.org/10.1021/am505036a>
- Chi Y, Chou P-T (2010) Transition-metal phosphors with cyclometalating ligands: fundamentals and applications. *Chem Soc Rev* 39:638–655. <https://doi.org/10.1039/B916237B>
- Chikamatsu M, Itakura A, Yoshida Y, Azumi R, Yase K (2008) High-performance n-type organic thin-film transistors based on solution-processable perfluoroalkyl-substituted C₆₀ derivatives. *Chem Mater* 20:7365–7367. <https://doi.org/10.1021/cm802577u>
- de la Cruz C, Molina A, Patil N, Ventosa E, Marcilla R, Mavrandonakis A (2020) New insights into phenazine-based organic redox flow batteries by using high-throughput DFT modelling. *Sustain Energy Fuels* 4:5513–5521. <https://doi.org/10.1039/d0se00687d>
- Doré K, Dubus S, Ho HA, Lévesque I, Brunette M, Corbeil G, Boissinot M, Boivin G, Bergeron MG, Boudreau D, Leclerc M (2004) Fluorescent polymeric transducer for the rapid, simple, and specific detection of nucleic acids at the zeptomole level. *J Am Chem Soc* 126:4240–4244. <https://doi.org/10.1021/ja038900d>
- Durban MM, Kazarino PD, Segawa Y, Luscombe CK (2011) Synthesis and characterization of solution-processable ladderized n-type naphthalene bisimide copolymers for OFET applications. *Macromolecules* 44:4721–4728. <https://doi.org/10.1021/ma2004822>
- Friend RH, Gymer RW, Holmes AB, Burroughes JH, Marks RN, Taliani C, Bradley DDC, Dos Santos DA, Brédas JL, Lögdlund M, Salaneck WR (1999) Electroluminescence in conjugated polymers. *Nature* 397:121–128. <https://doi.org/10.1038/16393>
- Frisch MJ, Trucks GW, Schlegel HB, Scuseria GE, Robb MA, Cheeseman JR, Montgomery JA Jr, Vreven T, Kudin KN, Burant JC, Millam JM, Iyengar SS, Tomasi J, Barone V, Mennucci B, Cossi M, Scalmani G, Rega N, Petersson GA, Nakatsuji H, Hada M, Ehara M, Toyota K, Fukuda R, Hasegawa J, Ishida M, Nakajima T, Honda Y, Kitao O, Nakai H, Klene M, Li X, Knox JE, Hratchian HP, Cross JB, Bakken V, Adamo C, Jaramillo J, Gomperts R, Stratmann RE, Yazyev O, Austin AJ, Cammi R, Pomelli C, Ochterski JW, Ayala PY, Morokuma K, Voth GA, Salvador P, Dannenberg JJ, Zakrzewski VG, Dapprich S, Daniels AD, Strain MC, Farkas O, Malick DK, Rabuck AD, Raghavachari K, Foresman JB, Ortiz JV, Cui Q, Baboul AG, Clifford S, Cioslowski J, Stefanov BB, Liu G, Liashenko A, Piskorz P, Komaromi I, Martin RL, Fox DJ, Keith T, Al-Laham MA, Peng CY, Nanayakkara A, Challacombe M, Gill PMW, Johnson B, Chen W, Wong MW, Gonzalez C, Pople JA (2004) Gaussian, 03, Revision C02. Gaussian Inc, Wallingford CT.
- Furue R, Nishimoto T, Park I-S, Lee J, Yasuda T (2016) Aggregation-induced delayed fluorescence based on donor/acceptor-tethered janus carborane triads: unique photophysical properties of non-doped OLEDs. *Angew Chem Int Ed* 55:7171–7175. <https://doi.org/10.1002/anie.201603232>
- Gao X, Hu Y (2014) Development of n-type organic semiconductors for thin film transistors: a viewpoint of molecular design. *J Mater Chem C* 2:3099–3017. <https://doi.org/10.1039/c3tc32046d>
- Grätzel M (2009) Recent advances in sensitized mesoscopic solar cells. *Acc Chem* 42:1788–1798. <https://doi.org/10.1021/ar900141y>
- Havare A (2020) Analysis of ITO surface modified with aromatic-based self-assembled molecules. *Bull Mater Sci* 43:266. <https://doi.org/10.1007/s12034-020-02178-4>
- He Y, Yagi S, Maeda T, Nakazumi H, Yagi S (2015) Synthesis and luminescent properties of novel Dibenzo[*a, c*]phenazine derivatives with electron-donating side-arms. *Mol Cryst Liq Cryst* 621:64–69. <https://doi.org/10.1080/15421406.2015.1095927>
- Hong Y, Lam JWY, Tang BZ (2011) Aggregation-induced emission. *Chem Soc Rev* 40:5361–5388. <https://doi.org/10.1039/C1CS15113D>
- Huang J, Sun N, Yang J, Tang R, Li Q, Ma Q, Zheng L (2014) Blue aggregation-induced emission luminogens: high external quantum efficiencies up to 3.99% in LED device, and restriction of the conjugation length through rational molecular design. *Adv Funct Mater* 48:7645–7654. <https://doi.org/10.1002/adfm.201401867>
- Hung LS, Chen CH (2002) Recent progress of molecular organic electroluminescent materials and devices. *Mat Sci Eng R Rep* 39:143–222. [https://doi.org/10.1016/S0927-796X\(02\)00093-1](https://doi.org/10.1016/S0927-796X(02)00093-1)

- Imahori H, Umeyama T, Ito S (2009) Large π -aromatic molecules as potential sensitizers for highly efficient dye-sensitized solar cells. *Acc Chem Res* 42:1809–1818. <https://doi.org/10.1021/ar900034t>
- Jiao GS, Thoresen LH, Burgess K (2003) Fluorescent, through-bond energy transfer cassettes for labeling multiple biological molecules in one experiment *J Am Chem Soc* 1226:14668–14669. <https://doi.org/10.1021/ja0371931>
- Jones BA, Facchetti A, Wasielewski MR, Marks TJ (2007) Tuning orbital energetics in arylene diimide semiconductors. Materials design for ambient stability of n-type charge transport. *J Am Chem Soc* 129:15259–15278. <https://doi.org/10.1021/ja075242e>
- Jung HS, Verwilt P, Kim WY, Kim JS (2016) Fluorescent and colorimetric sensors for the detection of humidity or water content. *Chem Soc Rev* 45:1242–1256. <https://doi.org/10.1039/c5cs00494b>
- Kamble RM, Sharma BK, Shaikh AM, Chacko S (2018) Design, synthesis, opto-electrochemical and theoretical investigation of novel indolo[2,3-*b*]naphtho[2,3-*f*] quinoxaline derivatives for n-type materials in organic electronics. *ChemistrySelect* 3:6907–6915. <https://doi.org/10.1002/slct.201801208>
- Kanekar DN, Chacko S, Kamble RM (2018) Synthesis, opto-electrochemical and theoretical investigation of pyrazino[2,3-*b*]phenazine amines for organic electronics. *ChemistrySelect* 3:4114–4123. <https://doi.org/10.1002/slct.201800562>
- Kanekar DN, Chacko S, Kamble RM (2019) Quinoxaline based amines as Blue-orange emitters: effect of modulating donor system on Optoelectrochemical and theoretical properties. *Dye Pigments* 167:36–50. <https://doi.org/10.1016/j.dyepig.2019.04.005>
- Kanekar DN, Chacko S, Kamble RM (2020) Synthesis and investigation of the photophysical, electrochemical and theoretical properties of phenazine–amine based cyan blue-red fluorescent materials for organic electronics. *New J Chem* 44:3278–3293. <https://doi.org/10.1039/c9nj06109f>
- Kasai H, Nalwa HS, Oikawa H, Okada S, Matsuda H, Minami N, Kakuta A, Ono K, Mukoh A, Nakanishi H (1992) A novel preparation method of organic microcrystals. *Jpn J Appl Phys* 31:L1132–L1134. <https://doi.org/10.1143/JJAP.31.L1132>
- Lakowicz JR (2006) Solvent and environmental effects. In: Lakowicz JR. (eds) Principles of fluorescence spectroscopy. Boston, MA: Springer. <https://doi.org/10.1007/978-0-387-46312-4>
- Lee BL, Yamamoto T (1999) Syntheses of new alternating CT-type copolymers of thiophene and pyrido[3,4-*b*]pyrazine units: their optical and electrochemical properties in comparison with similar CT copolymers of thiophene with pyridine and quinoxaline. *Macromolecules* 32:1375–1382. <https://doi.org/10.1021/ma981013o>
- Liu W, Ying S, Zhang Q, Ye S, Guo R, Ma D, Wang L (2018) New multifunctional aggregation-induced emission fluorophores for reversible piezofluorochromic and nondoped sky-blue organic light-emitting diodes. *Dye Pigments* 158:204–212. <https://doi.org/10.1016/j.dyepig.2018.05.030>
- Mahadik SS, Chacko S, Kamble RM (2019) 2,3-Di(thiophen-2-yl) quinoxaline amine derivatives: yellow-blue fluorescent materials for applications in organic electronics *ChemistrySelect* 4:10021–10032. <https://doi.org/10.1002/slct.201902109>
- Mahadik SS, Garud DR, Ware AP, Pingale SS, Kamble RM (2021) Design, synthesis and opto-electrochemical properties of novel derivatives as blue-orange fluorescent materials. *Dye Pigments* 184:108742. <https://doi.org/10.1016/j.dyepig.2020.108742>
- Mattaga N, Kaifu Y, Koizumi M (1956) Solvent effects upon fluorescence spectra and the dipole moments of excited molecules. *Bull Chem Soc Jpn* 29:465–470. <https://doi.org/10.1246/bcsj.29.465>
- Meijer EJ, de Leeuw DM, Setayesh S, Veenendaal E-V, Huisman BH, Blom PW, Hummelen JC, Scherf U, Kadam J, Klapwijk TM (2003) Solution-processed ambipolar organic field-effect transistors and inverters. *Nat Mater* 2:678–682. <https://doi.org/10.1038/nmat978>
- Misra A, Kumar L, Kumar P, Dhawan SK, Kamalasanan MN, Chandra S (2004) Blue electroluminescence in organic semiconductors. *Indian J Pure Ap Phy* 42:793–805. ISSN:0019–5596
- Misra R, Bhattacharyya SP (2018) Intramolecular charge transfer: theory and applications, Weinheim, Germany: Wiley. <https://doi.org/10.1002/9783527801916>
- Miyaura N, Yanagi T, Suzuki A (1981) The palladium-catalyzed cross-coupling reaction of phenylboronic acid with haloarenes in the presence of bases. *Synth Commun* 11:513–519
- Miyaura N (2002) Cross-coupling reactions: a practical guide. Springer, New York, p 248
- Mullen K, Scherf U (2006) Organic light-emitting devices: synthesis, properties and applications, Weinheim: Wiley
- Negishi EA (2002) Handbook of organopalladium chemistry for organic synthesis. Wiley, New York
- Okamoto T, Terada E, Kozaki M, Uchida M, Kikukawa S, Okada K (2003) Facile synthesis of 5,10-diaryl-5,10-dihydrophenazines and application to EL devices. *Org Lett* 5:373–376. <https://doi.org/10.1021/ol20274458>
- Otsuki S, Adachi K (1993) Effect of humidity on the fluorescence properties of a medium sensitive fluorophore in a hydrophilic polymer film. *J Photochem Photobiol* 71:169–173. [https://doi.org/10.1016/1010-6030\(93\)85069-K](https://doi.org/10.1016/1010-6030(93)85069-K)
- Qin W, Zhiyong Y, Yibin J, Lam JWY, Liang G, Kwok HS, Tang BZ (2015) Construction of efficient deep blue aggregation-induced emission luminogen from triphenylethene for non-doped organic light-emitting diodes. *Chem Mater* 27:3892–3901. <https://doi.org/10.1021/acs.chemmater.5b00568>
- Reichardt C (2002). Empirical parameters of solvent polarity. In: Reichardt C (ed) Solvents and solvent effects in organic chemistry, 3rd ed, Weinheim: Wiley-VCH. <https://doi.org/10.1002/3527601791.ch7>
- Shaikh AM, Sharma BK, Chacko S, Kamble RM (2016) Synthesis and optoelectronic investigations of triaryl amines based on naphtho[2,3-*f*]quinoxaline-7,12-dione core as donor–acceptors for n-type materials *RSC Adv* 6:60084–60093. <https://doi.org/10.1039/C6RA11149A>
- Shaikh AM, Sharma BK, Chacko S, Kamble RM (2016b) Synthesis and opto-electrochemical properties of tribenzo[*a, c, i*]phenazine derivatives for hole transport materials. *RSC Adv* 6:94218–94227. <https://doi.org/10.1039/C6RA20964E>
- Shaikh AM, Sharma BK, Chacko S, Kamble RM (2017) Novel electroluminescent donor–acceptors based on dibenzo[*a, c*]phenazine as hole-transporting materials for organic electronics. *New J Chem* 41:628–638. <https://doi.org/10.1039/c6nj03553a>
- Shaikh AM, Sharma BK, Kamble RM (2015) Synthesis, photophysical, electrochemical and thermal studies of triaryl amines based on benzo[*g*]quinoxalines. *J Chem Sci* 127:1571–1579. <https://doi.org/10.1007/s12039-015-0904-0>
- Shaikh AM, Sharma BK, Kamble RM (2016c) Electron-deficient molecules: photophysical, electrochemical, and thermal investigations of naphtho[2,3-*f*]quinoxaline-7,12-dione derivatives. *Chem Heterocycl Compd* 52:110–115. <https://doi.org/10.1007/s10593-016-1842-6>
- Sharma BK, Shaikh AM, Chacko S, Kamble RM (2017) Synthesis, spectral, electrochemical and theoretical investigation of indolo[2,3-*b*]quinoxaline dyes derived from Anthraquinone for n-type materials. *J Chem Sci* 129:483–494. <https://doi.org/10.1007/s12039-017-1252-z>
- Singh PS, Badani PM, Kamble RM (2019a) Impact of the donor substituent on the optoelectrochemical properties of 6*H*-indolo[2,3-*b*]quinoxaline amine derivatives. *New J Chem* 43:19379–19396. <https://doi.org/10.1039/c9nj05558d>
- Singh PS, Chacko S, Kamble RM (2019) The design and synthesis of 2,3-diphenylquinoxaline amine derivatives as yellow-blue

- emissive materials for optoelectrochemical study. *New J Chem* 43:6973–6988. <https://doi.org/10.1039/C9NJ00248K>.
- Staub K, Levina GA, Barlow S, Kowalczyk TC, Lackritz HS, Fort A, Marder SR (2003) Synthesis and stability studies of conformationally locked 4-diarylaminoaryl- and 4-dialkylaminophenyl-substituted second-order nonlinear optical polyene chromophores. *J Mater Chem* 13:825–833. <https://doi.org/10.1039/B208024A>
- Sun SS, Sariciftci NS (2005) Organic photovoltaics: mechanism, materials, devices, Taylor and Francis, United States
- Thomas KRJ, Lin JT, Tao YT, Chuen CH (2002) Quinoxalines incorporating Triarylamines: potential electroluminescent materials with tunable emission characteristics. *Chem Mater* 14:2796–2802. <https://doi.org/10.1021/cm0201100>
- Tong H, Dong Y, Haubler M, Lam JWY, Sung Y, Williams ID, Sun J, Tang B (2006) Tunable aggregation-induced emission of diphenyldibenzo fulvenes. *Chem Commun* 10:1133–1135. <https://doi.org/10.1039/B515798F>
- Von Lippert E (1957) Spektroskopische bistimmung des dipolmomentes aromatischer verbindungen im ersten angeregten singuletzustand. *Z Electrochem* 61:962–975. <https://doi.org/10.1002/bbpc.19570610819>
- Wang Z, Song X, Ma L, Feng Y, Gu C, Zhang X (2013) A triphenylamine-capped solution-processable wholly aromatic organic molecule with electrochemical stability and its potential application in photovoltaic devices. *New J Chem* 37:2440–2447. <https://doi.org/10.1039/C3NJ00406F>
- Weller A (1956) Intramolecular proton transfer in excited states. *Angew Phys Chem* 60:1144–1147. <https://doi.org/10.1002/bbpc.19560600938>
- Winkler M, Houk KN (2007) Nitrogen-rich oligoacenes: candidates for n-channel organic semiconductor. *J Am Chem Soc* 129:1805–1815. <https://doi.org/10.1021/ja067087u>
- Xie FM, Wu P, Zou SJ, Li YQ, Cheng T, Xie M, Tang JX, Zhao X (2020) Efficient orange–red delayed fluorescence organic light-emitting diodes with external quantum efficiency over 26%. *Adv Electron Mater* 6:1900843. <https://doi.org/10.1002/aelm.201900843>
- Xu L, Zhao Y, Long G, Wang Y, Zhao J, Li D, Li J, Ganguly R, Li Y, Sun H, Sun XW, Zhang Q (2015a) Synthesis, structure, physical properties and OLED application of pyrazine–triphenylamine fused conjugated compounds. *RSC Adv* 5:63080–63086. <https://doi.org/10.1039/C5RA12654A>
- Xu L, Zhu H, Long G, Zhao J, Li D, Ganguly R, Li Y, Xu Q-H, Zhang Q (2015b) Diphenylamino-phenyl substituted pyrazine: nonlinear optical switching by protonation. *J Mater Chem C* 3:9191–9196. <https://doi.org/10.1039/C5TC01657F>
- Yuan WZ, Lu P, Chen S, Lam JWY, Wang Z, Liu Y, Kwok HS, Ma Y, Tang BZ (2010) Changing the behavior of chromophores from aggregation-caused quenching to aggregation-induced emission: development of highly efficient light emitters in the solid state. *Adv Mater* 22:2159–2163. <https://doi.org/10.1002/adma.200904056>
- Zheng Z, Dong Q, Gou L, Su J-H, Huang J (2014) Novel hole transport materials based on N, N'-disubstituted-dihydrophenazine derivatives for electroluminescent diodes. *J Mater Chem C* 2:9858–9865. <https://doi.org/10.1039/C4TC01965B>
- Zhou K, Dong H, Zhang H, Hu W (2014) High performance n-type and ambipolar small organic semiconductors for organic thin film transistors. *Phys Chem Chem Phys* 16:22448–22457. <https://doi.org/10.1039/C4CP01700E>
- Zhou L, Mao J, Ren Y, Vellaisamy S-TH, Roy AL, Zhou Y (2018) Recent advances of flexible data storage devices based on organic nanoscaled materials. *Small* 1703126:1–27. <https://doi.org/10.1002/smll.201703126>

Publisher's Note Springer Nature remains neutral with regard to jurisdictional claims in published maps and institutional affiliations.

Authors and Affiliations

Deepali N. Kanekar¹ · Purav M. Badani¹ · Rajesh M. Kamble¹ 

✉ Rajesh M. Kamble
kamblerm@chem.mu.ac.in

¹ Department of Chemistry, University of Mumbai, Santacruz (E), Mumbai 400098, India